Proc. Natl. Acad. Sci. USA
Vol. 88, pp. 2588–2592, March 1991
Biophysics

Nature and functional implications of the cytochrome a_3 transients after photodissociation of CO–cytochrome oxidase

(time-resolved spectroscopy/heme and copper ligation/ligand shuttle/proton translocation)

WILLIAM H. WOODRUFF*†, ÓLÖF EINARSDÓTTIR§, R. BRIAN DYER¶, KIMBERLY A. BAGLEY*, GRAHAM PALMER‖, STEPHEN J. ATHERTON**, ROBERT A. GOLDBECK§, TIMOTHY D. DAWES§, AND DAVID S. KLIGER§

*INC-4, Mail Stop C345, and ¶CLS-4, Mail Stop J567, Los Alamos National Laboratory, Los Alamos, NM 87545; §Department of Chemistry, University of California, Santa Cruz, CA 95064; ‖Department of Biochemistry, Rice University, Houston, TX 77251; and **Center for Fast Kinetics Research, The University of Texas at Austin, Austin, TX 78712

Communicated by Harry B. Gray, September 18, 1990

ABSTRACT **Time-resolved electronic absorption, infrared, resonance Raman, and magnetic circular dichroism spectroscopies are applied to characterization of the intermediate that is formed within 20 ps after photodissociation of CO from cytochrome a_3 in reduced cytochrome oxidase. This intermediate decays with the same half-life ($\approx$1 μs) as the post-photodissociation Cu_B^+–CO species previously observed by time-resolved infrared. The transient UV/visible spectra, kinetics, infrared, and Raman evidence suggest that an endogenous ligand is transferred from Cu_B to Fe_{a3} when CO binds to Cu_B, forming a cytochrome a_3 species with axial ligation that differs from the reduced unliganded enzyme. The time-resolved magnetic circular dichroism results suggest that this transient is high-spin and, therefore, five-coordinate. Thus we infer that the ligand from Cu_B binds on the distal side of cytochrome a_3 and displaces the proximal histidine imidazole. This remarkable mechanistic feature is an additional aspect of the previously proposed "ligand-shuttle" activity of the Cu_B/Fe_{a3} pair. We speculate as to the identity of the ligand that is transferred between Cu_B and Fe_{a3} and suggest that the ligand shuttle may play a functional role in redox-linked proton translocation by the enzyme.**

In a recent time-resolved infrared (TRIR) study (1) of the events after photodissociation of CO from cytochrome (cyt) a_3 of reduced beef heart cytochrome oxidase (CcO), we reported conclusive evidence that photodissociated CO binds quantitatively to Cu_B^+ at room temperature prior to equilibrating with solution. In a parallel kinetics study (Ó.E., P. M. Killough, R.B.D., J. J. López-Garriga, S. M. Hubig, S.J.A., G.P., and W.H.W., unpublished data), we have shown that the pathway for CO in solution to its binding site on Fe_{a3}^{2+}

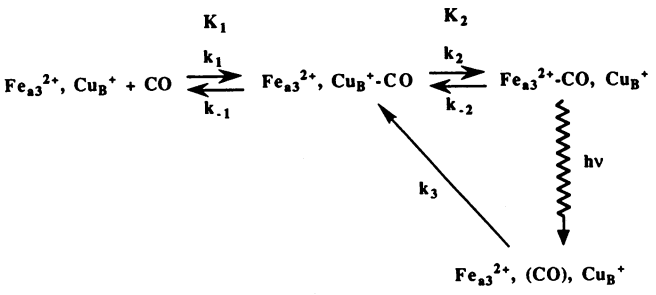

Scheme I

likewise involves a Cu_B^+–CO intermediate. This mechanism is depicted in Scheme I above. In this scheme K_1 and k_2 are 130 M^{-1} and 700 s^{-1}, respectively (Ó.E. *et al.*, unpublished data).

By using TRIR, we have determined k_{-1} to be 4.7×10^5 s^{-1} (1). These results reveal that Cu_B^+, in addition to its established electron transfer role, functions as a "ligand shuttle" in transporting CO (and plausibly other exogenous ligands including O_2) to and from the heme of cyt a_3. In this report we present time-resolved spectroscopic results that suggest that, during the lifetime of the Cu_B^+–CO complex, the cyt a_3 heme differs from the five-coordinate, imidazole-liganded, high-spin structure that it assumes in the reduced unliganded enzyme. We suggest that binding of CO to Cu_B^+ triggers the transfer of an endogenous ligand, which we denote L, from Cu_B^+ to Fe_{a3}^{2+}. The probes that we have applied to characterization of this transient (ref. 1 and Ó.E. *et al.*, unpublished data and the present work) include electronic absorbance [UV/Visible (UV/Vis)], which establishes the kinetics of the heme absorbance changes; infrared absorbance (TRIR), which establishes the kinetics and structure of the Cu_B^+–CO intermediate (1); time-resolved resonance Raman (TR^3), which provides evidence on heme structure and axial ligation; and time-resolved magnetic circular dichroism (TRMCD), which gives information on the transient spin states of cyt a_3. The results suggest that L, in binding to cyt a_3 on the distal side, displaces the proximal histidine resulting in a transient five-coordinate species, Fe_{a3}–L. Furthermore, it appears that L is not imidazole. Given the similar properties of O_2 and CO as ligands, it seems probable that similar ligand-shuttle phenomena may accompany the coordination of O_2 before its reduction and may play a role in the functional dynamics of the enzyme.

MATERIALS AND METHODS

CcO was prepared and handled as described elsewhere (Ó.E. *et al.*, unpublished data; ref. 3). The UV/Vis samples were 10 μM or 55 μM in total heme A, and the TR^3 samples were 240 μM. Specific experimental details of TRIR, TRMCD, kinetic UV/Vis, and TR^3 measurements are provided elsewhere (1–8).

RESULTS AND DISCUSSION

Transient Absorbance. By using UV/Vis measurements between 100 fs and 100 ms, we have studied the photodissociation/recombination reactions of CcO–CO (Ó.E. *et al.*, unpublished data; P. O. Stoutland, J.-C. Lambry, J.-L. Martin, and W.H.W., unpublished data). During rebinding of CO on the millisecond timescale, the transient difference features

The publication costs of this article were defrayed in part by page charge payment. This article must therefore be hereby marked "*advertisement*" in accordance with 18 U.S.C. §1734 solely to indicate this fact.

Abbreviations: TRIR, time-resolved infrared; CcO, cytochrome oxidase; TRMCD, time-resolved magnetic circular dichroism; UV/Vis, UV/visible; TR^3, time-resolved resonance Raman; cyt, cytochrome.

†To whom reprint requests should be addressed.

created by photodissociation return to $\Delta A = 0$ with the observed rate constant k_{obs}. The value of k_{obs} is a function of CO concentration, and its dependence upon [CO] yields K_1 and k_2 in Scheme I (Ó.E. *et al.*, unpublished data). On shorter time scales the α band shows two additional transients. The first, which appears as an increase in absorbance at 610 nm with a half-life of 20 ps, has a contribution from cyt *a*; the actual rise time of the cyt a_3 transient is 20 ps or less (P. O. Stoutland *et al.*, unpublished data). By comparison, the rise time of the Cu_B–CO absorbance measured by TRIR is 1 ps or less (9). The second UV/Vis transient is a 25% decrease in ΔA at 610 nm between 100 ns and 10 μs ($k = 8 \times 10^5\ s^{-1}$). Given the respective experimental conditions (ref. 1; Ó.E. *et al.*, unpublished data), we consider this to be the same as the $5 \times 10^5\ s^{-1}$ rate constant observed by TRIR for loss of CO by Cu_B^+–CO (k_{-1} in Scheme I) (1).

Despite the relationship in time between the α-band transient and the dissociation of Cu_B–CO, it is most unlikely that the observed changes in the heme absorption spectrum could be directly due to changes in the coordination sphere of Cu_B^+. Instead it is probable that the binding and dissociation of CO at Cu_B^+ indirectly causes a change in structure at the heme which in turn is directly responsible for the absorbance changes. We infer from results presented in the following discussion that the structural change in question involves changes in cyt a_3 axial ligation (i.e., transfer of the ligand L from Cu_B^+ to cyt a_3) triggered by binding of photodissociated CO to Cu_B^+. Conversely, we suggest that the microsecond-time-scale event causing the diminution in α-band intensity is the return of L from cyt a_3 to Cu_B, triggered by loss of CO from Cu_B^+–CO into solution. The UV/Vis absorption changes allow several different interpretations as to the ligation and spin state of the heme. Choice among these alternatives requires evidence from other, more structure-specific approaches (*vide infra*).

Kinetics and Photolability. We have determined that the rate constant k_2 for transfer of CO from Cu_B^+ to Fe_{a3}^{2+} is 700 s^{-1} (Ó.E. *et al.*, unpublished data). The rate-determining step for this reaction cannot be loss of CO by Cu_B, which we have shown by TRIR to be at least 1000 times faster (1). Furthermore, this rate cannot be limited by the intrinsic dynamics of a five-coordinate heme; typical geminate CO-rebinding reactions of heme proteins have half-lives on the nanosecond time scale (10). The protein has clearly erected a substantial barrier to heme–CO rebinding after the photodissociation of CO and its binding to Cu_B. We suggest that this barrier is introduced by the transfer of L to the former CO-binding site on the heme, triggered by binding of CO to Cu_B. L remains bound to the heme for the lifetime of the Cu_B–CO complex, thus preventing the return of CO. The rate-determining step for transfer of CO to Fe_{a3}^{2+} is then the breaking of the Fe–L bond. A thermal bond dissociation rate in the vicinity of 1000 s^{-1} is consistent with known axial bond dissociation rates of either six-coordinate low-spin or five-coordinate high-spin hemes (11), but a factor of 100–1000 slower than the rate expected of six-coordinate high-spin ferrous complexes (12).

During our kinetics studies (Ó.E. *et al.*, unpublished data), we observed that the recombination of CO with cyt a_3 is accelerated by increasing the probe light intensity of the transient spectrophotometer. It is remarkable that the formation of the heme–CO complex, which is itself photodissociable, is made faster by increased light intensity. However, this is easily understood in the mechanism suggested above. If breaking of the Fe–L bond is the rate determining step for the return of CO to the heme and if the Fe–L bond is photolabile (13), light will accelerate both k_2 and k_{obs}.

TR³. Previous TR^3 studies (14) have suggested that the cyt a_3 intermediate that forms after photodissociation and persists for $\approx$1 μs is an essentially normal high-spin five-coordinate imidazole-liganded species, albeit with a somewhat high Fe–N(imidazole) stretching frequency. It is now clear (Ó.E. *et al.*, unpublished data) that these earlier studies would not have detected the Fe_{a3}–L species; this intermediate would have been photodissociated by the probe laser pulse energies used. Fig. 1 shows TR^3 spectra obtained at pulse-probe time delay of 200 ns; the high- and low-frequency regions are both shown. The upper traces employ relatively high probe laser pulse energy (1 mJ) and the lower traces employ low-energy probe pulses ($\approx$10 μJ). In the high-frequency region, some diminution in intensity of the high-spin indicator band (1572 cm^{-1}) may occur at low probe pulse energy. At the same time, the oxidation state marker peak appears unchanged in frequency and line shape at 1356 cm^{-1} in the two traces. This demonstrates that the spectrum in the low-power trace is not due to the CO complex, which would show an oxidation state marker peak at $\approx$1372 cm^{-1} (15). In the low-frequency region, the high-power trace clearly shows the Fe–N(Im) stretch of five-coordinate high-spin cyt a_3 at 223 cm^{-1}, as in the earlier TR^3 study (14). However, this peak is greatly reduced in the low-power trace.

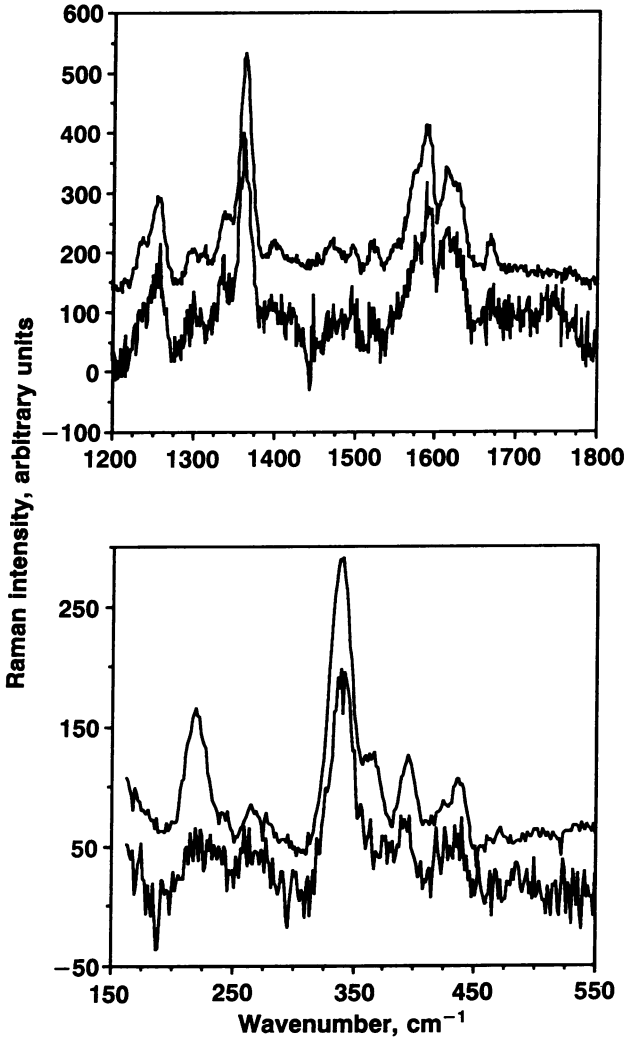

FIG. 1. TR^3 spectra obtained 200 ns after photodissociation of CO from fully reduced CcO. (*Upper*) High-frequency region of the Raman spectrum (1200–1800 cm^{-1}). (*Lower*) Low-frequency region (150–550 cm^{-1}). The upper spectra are obtained with probe laser pulses of $\approx$1-mJ energy (442 nm, $\approx$5-ns duration) and the lower spectra are obtained with $\approx$10-μJ pulse energy.

There are two tenable interpretations of the TR^3 results. First, the low-power TR^3 spectrum may be due to a six-coordinate low-spin species with both L and imidazole as axial ligands. In general, the Fe–N(Im) stretching peak is

missing from the resonance Raman (RR) spectra of six-coordinate low-spin heme complexes (16). In this interpretation the photolability of the Fe–L bond accounts for the typical five-coordinate high-spin spectrum observed at high laser pulse energies; L may be imidazole itself or other ligands that are relatively poor π-acids. Alternatively, the low-power TR^3 spectrum may be due to a five-coordinate high-spin cyt a_3–L complex wherein L is not imidazole and has properties that induce cleavage of the Fe_{a3}–N(proximal histidine) bond. In this interpretation the disappearance of the 223-cm^{-1} peak occurs simply because the axial ligand L is not imidazole. Photodissociation of L by the probe laser pulse allows photostationary rebinding of the proximal histidine and regeneration of an essentially normal high-spin Raman spectrum.

A six-coordinate high-spin imidazole–heme–L transient is allowed by our data but is considered unlikely for several reasons including the spectroscopic and kinetics evidence cited above and the absence of any ferrous heme models that are high-spin and six-coordinate with imidazole as one of the axial ligands (17, 18).

TRMCD. The MCD spectrum of reduced unliganded CcO has a large contribution from the signal due to high-spin cyt a_3. This is characterized by an intense positive Soret MCD feature at 455 nm (see Fig. 2); the contribution of low-spin cyt a is approximately the spectrum of CcO–CO, which has a negligible contribution from cyt a_3–CO (19). If the cyt a_3 transient is six-coordinate and low-spin, the positive high-spin MCD signal at 455 nm should grow in the TRMCD spectrum as the low-spin intermediate disappears with a half-life of $\approx$1 μs. This is not the case; instead a MCD signal that is similar to that of unliganded CcO develops within the excitation laser pulse width ($\leq$10 ns). This spectrum is replaced by that of CcO–CO on the millisecond time scale. Fig. 2 shows the 200-ns and 10-μs TRMCD spectra; the ground-state MCD spectra of unliganded CcO and CcO–CO are included for comparison. Both of the TRMCD spectra (200 ns and 10 μs), although slightly different from one another, are as expected of a high-spin cyt a_3 species. Although the caveat must be made that MCD spectra of model intermediate-spin ferrous hemes have not been determined, the TRMCD results are strong evidence that the transient observed in the UV/Vis and TR^3 experiments is not low-spin and is probably high-spin.

Nature of the 10-ps to 1-μs Transient and Possible Identity of Ligand L. The evidence presented above favors a structure for the post-photodissociation transient wherein CO is bound to Cu_B, L is released and binds to cyt a_3 on the distal side, and

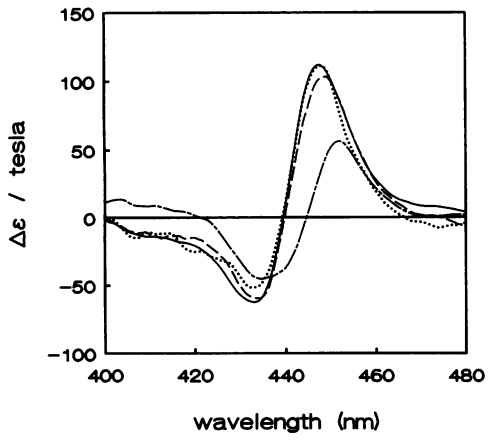

FIG. 2. MCD spectra of fully reduced unliganded CcO (solid line) and its CO derivative (- - - -). TRMCD spectra of the photodissociated CO–enzyme were obtained 200 ns (---) and 10 μs (·····) after photodissociation of CO from the heme.

the bond between the heme iron and the proximal histidine is broken. The UV/Vis kinetics (Ó.E. *et al.*, unpublished data) set the time scales for the binding of L to the heme ($\leq$20 ps) and its return to Cu_B ($\approx$1 μs) as CO binds to Cu_B ($\leq$1 ps) and dissociates into solution ($\approx$1 μs) (1, 9). The TRMCD suggests that the transient is high-spin and, therefore, five-coordinate. Whereas we cannot definitively reject a six-coordinate high-spin structure, this seems an unlikely alternative based upon arguments developed in preceding sections.

Alternative possibilities exist. One is that L is never bound to Cu_B but simply binds to the heme upon photodissociation of CO. If this were the case, there appears to be no reason why L should not bind to Fe^{2+}_{a3} in the reduced unliganded enzyme. A second is that L is not present at all. In the second scenario, the binding of CO to Cu_B triggers a protein conformational change that changes the UV/Vis and Raman spectra of cyt a_3 and also blocks the pathway of CO from Cu_B to the heme on the distal side without ligating the heme. This does not, however, account for photoacceleration of the rebinding of CO to the heme, the photosensitivity of the TR^3 spectra, or the absence of the Fe–N(Im) stretching peak in the TR^3 spectra. Nor is a large conformational change supported by the activation parameters for k_2, which are temperature independent from 140 K to 300 K (Ó.E. *et al.*, unpublished data).

We cannot determine the identity of L from the present evidence, but we may speculate based upon its characteristics that we now summarize. The Cu^+_B–CO bond must be more stable than the Cu^+_B–L bond. In the absence of CO, Cu(I)–L is more stable than Fe(II)–L. The Fe^{2+}_{a3}–L bond on the distal side of the heme must be more stable than the Fe^{2+}_{a3}–(proximal histidine) bond. In addition L must have steric or electronic properties that do not permit it to bind to Fe^{2+}_{a3} trans to the proximal histidine without breaking the Fe–N(Im) bond (this property has been observed, for example, for NO bound to T-state hemoglobin; see ref. 20). These are restrictive criteria that are not obviously met by amino acid side chains that commonly ligate metal ions in proteins, except perhaps thiolate from cysteine. Nor are they met by peptide ligands or by common exogenous ligands such as H_2O, OH^-, O^{2-}, Cl^-, etc.

Thiolate ligands bind to ferrous porphyrins to form five-coordinate high-spin complexes (17) and are good ligands for Cu(I). Coordination of a second-row ligand (Cl^- or RS^-) is implicated in the extended x-ray absorption fine structure (EXAFS), of resting CcO (21). Thus cysteine thiolate might be a reasonable candidate for L. However, it is not clear whether RS^- will displace imidazole from ferrous hemes, as required by the criteria above. More importantly, primary structure comparisons of subunit 1 of mammalian CcO with oxidases from other species (22) indicate that this polypeptide lacks conserved cysteine residues.

An intriguing though unorthodox alternative to RS^- as a candidate for L is presented by the unsaturated isoprenoid groups of the farnesyl tail of heme A. Copper(I)–olefin coordination is common in organometallic chemistry, and iron(II) and −(III) complexes of unsaturated groups are also well known (23, 24). Coordination options for ligands of this type include η_1 (σ-alkyl), η_2 (π-olefin), and η_3 (π-allyl). Coordination of the unsaturated tail of heme A to copper in CcO has been suggested (25–27), but binding to iron and the ligand shuttle role have not. The coordination of η_3 allyl to Fe^{2+} might meet the requirements for L including, in the square pyramidal geometry made obligatory by the heme, an intermediate or high-spin state (28). Steric interactions between axial π-allyl and the heme π system would probably require a large displacement of the iron toward the allyl, interfering with coordination of the proximal imidazole. These hypothetical structures are shown schematically below; the numbers correspond to the species in Fig. 3.

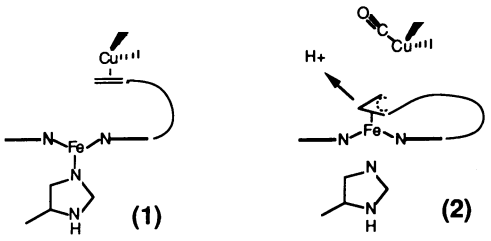

As indicated in structure 2 below, coordination of η_3 allyl to the heme requires deprotonation of the unsaturated group. Thus this "bioorganometallic" coordination chemistry could play a role in the proton-pumping function of the enzyme. In addition, it may be significant that valid η_3 allylic stuctures can be drawn at many points along the farnesyl chain. A role of η_3 allyl coordination in the oxidized forms of the enzyme and in mediating Cu–Fe interactions is also possible. Finally, we note the widespread presence of nonconjugated isoprenoid structures, namely in the unsaturated tail of ubiquinones, as elements of proton translocating systems in the mitochondrial electron transfer chain and other redox systems. We speculate that η_3 allylic coordination may play a significant and previously unsuspected role in redox-linked proton translocation.

CONCLUSIONS

The mechanism shown in Scheme I is insufficient to explain the observations described in the preceding sections. A minimal mechanism needed to account for the kinetics and the spectroscopic facts is shown in Fig. 3. The ligand L is exchanged between Cu_B^+ and Fe_{a3}^{2+} as CO binds to and dissociates from Cu_B. The binding of L to Fe_{a3} causes the release of the proximal histidine. The five-coordinate Fe_{a3}^{2+}–L complex, which is produced by routes that differ in detail depending upon whether CO dissociates thermally from the heme or the heme and the CO carry the excess energy of photoexcitation, is suggested to be responsible for the short timescale α-band transients and TRMCD spectrum, and the low-power TR^3 spectrum.

We expect that the phenomena observed in the coordination dynamics of CO are representative of the behavior of other similar π-acceptor ligands, including NO, isocyanides, and most importantly O_2. If this is the case, the ligand-shuttle activities of Cu_B^+ (*i*) in acting as an intermediate binding site for ligands entering and leaving the site of O_2 reduction, (*ii*) in synchronously transferring L between Cu_B and cyt a_3, and (*iii*) in engendering the release and rebinding of the proximal histidine imidazole undoubtedly have functional significance.

Since our initial reports of the ligand shuttle (1, 29, 30), results have appeared from other laboratories that support the view that these effects may be general and functionally important. In one of these studies, Raman spectral changes similar to those in the high-frequency region of Fig. 1 were observed upon energization of the membranes of reduced submitochondrial particles (31). This suggested axial ligation of cyt a_3 by an endogenous group, triggered by local pH change and/or conformational effects. Although the altered Raman spectrum was ascribed to a low-spin species (as we would have interpreted our Raman results in the absence of the TRMCD data), it is possible that the cyt a_3 heme ligation in the energized submitochondrial particles is the same as we infer for the submicrosecond transient in the CO photodis-

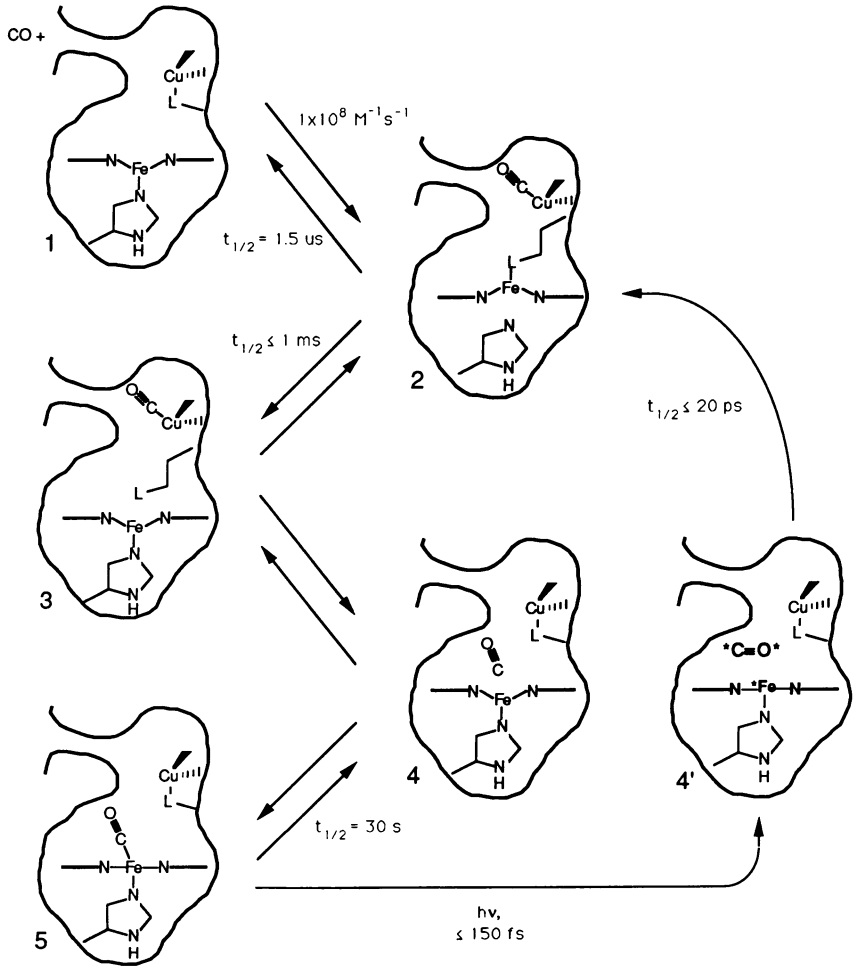

FIG. 3. Mechanism of CO binding to and dissociation from CcO, showing both thermal and photoinitiated reaction channels. Only Cu_B and Fe_{a3} are shown, and the protein structure is represented by the irregular line surrounding the metal centers. The species 1, 2, 3, 4, and 5 represent the thermal mechanism, and the species 4′ represents the geminate photoproduct. In 4′ the excess energy imparted to the heme and the CO as a consequence of photoexcitation is represented by the asterisks and the bold type. All of the half-lives are for first-order reactions, except for the photodissociation step and the bimolecular reaction with CO in solution; the half-lives are either known or reliably estimated from experiment, or else they are omitted.

sociation dynamics (Fig. 3, species 2). A second study (32) presents strong evidence that the species formed upon binding cyanide to fully oxidized CcO is not, as commonly believed, a Fe^{3+}_{a3}–(CN^-) complex but instead Cu^{+}_{B}–(CN^-). A possible interpretation of these results is that the binding of cyanide to Cu^{2+}_{B} triggers transfer of an endogenous ligand (*viz.*, the Fe–Cu bridging ligand in the oxidized enzyme, which may be identical with L) to Fe^{3+}_{a3}. A third study (J. R Schoonover and G.P., unpublished data) implicates labile ligation at Cu_B, and perhaps ligand exchange between Cu_B and Fe_{a3}, in the transition of resting CcO between its "fast" and "slow" forms.

The submitochondrial particle results cited above (31) provide a plausible experimental link between the ligand shuttle and proton translocation. We suggest that directed protonation/deprotonation reactions of L and the proximal histidine, accompanying the transfer of L from one metal to another on one side of the heme plane and the release and rebinding of the proximal histidine on the other, may act as microscopic "gates" for active proton translocation. This may occur whether L is the unsaturated group suggested in the preceding section, or any other ligand with a labile proton. The proton-gating mechanism based upon the ligand shuttle embodies the feature of being linked to the coordination chemistry of the Cu_B/Fe_{a3} pair, rather than exclusively to the redox reactivity. We emphasize that the thermodynamic driving force for proton translocation must arise from the energy of the electron transfer reactions associated with the reduction of O_2, as is commonly recognized (33–35). However, the ligand shuttle as a proton gate may be coupled to electron transfer in a very straightforward way, namely by changes in heme and copper redox potentials and electron transfer rates as a consequence of changing the identity or protonation state of the ligands. In this regard we note the recent result of Brzezinski and Malmström (2), who reported the electron transfer kinetics of mixed-valence CcO after photodissociation of CO from Fe^{2+}_{a3}, and established the rate constant for electron transfer from (Fe^{2+}_{a3}, Cu^{+}_{B}) to Cu^{2+}_{A} in the "E_1 state" to be 600 s^{-1} ($\Delta H‡$ = 7.7 kcal/mol and $\Delta S‡$ = −18 entropy units). By comparison we have measured the rate of dissociation of the Fe^{2+}_{a3}–L bond (k_2 in Scheme I or the conversion of intermediate 2 to 3 in Fig. 3) to be 700 s^{-1} ($\Delta H‡$ = 10.0 kcal/mol and $\Delta S‡$ = −12 entropy units) (Ó.E. *et al.*, unpublished data). The similarity of these kinetics parameters suggests that the rate-determining step for the electron-transfer reaction may be the cleavage of the Fe^{2+}_{a3}–L bond, that is, that the electron-transfer rate constant is much less than 600 s^{-1} when L is bound to Fe^{2+}_{a3} and much greater than 600 s^{-1} when L is free, such that Fe–L bond scission controls the electron transfer rate. Accordingly, it may be that a major microscopic difference between the E_1 and E_2 proton translocating states postulated by Brzezinski and Malmström (2, 35) is whether L is bound to Fe_{a3} or Cu_B.

This research was supported by National Institutes of Health Grant DK 36263 (W.H.W.), GM 38549 (D.S.K.), GM 21337 (G.P.), and RR 00886. Work at Los Alamos National Laboratory was performed under the auspices of the U.S. Department of Energy.

1. Dyer, R. B., Einarsdóttir, Ó., Killough, P. M., López-Garriga, J. J. & Woodruff, W. H. (1989) *J. Am. Chem. Soc.* **111**, 7657–7659.
2. Brzezinski, P. & Malmström, B. G. (1987) *Biochim. Biophys. Acta* **894**, 29–38.
3. Yoshikawa, S., Choc, M. G., O'Toole, M. C. & Caughey, W. S. (1977) *J. Biol. Chem.* **252**, 5498–5508.
4. Babcock, G. T., Jean, J. M., Johnston, L. N., Palmer, G. & Woodruff, W. H. (1984) *J. Am. Chem. Soc.* **106**, 8305–8306.
5. Varotsis, C., Woodruff, W. H. & Babcock, G. T. (1989) *J. Am. Chem. Soc.* **111**, 6439–6441.
6. Goldbeck, R. A., Dawes, T. D., Milder, S. J., Lewis, J. W. & Kliger, D. S. (1989) *Chem. Phys. Lett.* **156**, 545–549.
7. Kliger, D. S., Lewis, J. W. & Goldbeck, R. A. (1989) *SPIE J.* **1057**, 26–33.
8. Goldbeck, R. A., Dawes, T. D., Einarsdóttir, Ó., Woodruff, W. H. & Kliger, D. S. (1991) *Biochemistry*, in press.
9. Dyer, R. B., Peterson, K. A., Stoutland, P. O. & Woodruff, W. H. (1991) *J. Am. Chem. Soc.*, in press.
10. Martin, J.-L., Migus, A., Poyart, C., Lecarpentier, Y., Astier, R. & Antonetti, A. (1983) *Proc. Natl. Acad. Sci. USA* **80**, 173–178.
11. Shirazi, A., Barbush, M., Ghosh, S. & Dixon, D. W. (1985) *Inorg. Chem.* **24**, 2495–2502.
12. Eigen, M. & Wilkins, R. G. (1965) *Adv. Chem. Ser.* **49**, 55–80.
13. Jongeward, K. A., Megde, D., Taube, D. J. & Traylor, T. G. (1987) *J. Biol. Chem.* **263**, 6027–6030.
14. Findsen, E. W., Centeno, J., Babcock, G. T. & Ondrias, M. R. (1987) *J. Am. Chem. Soc.* **109**, 5367–5372.
15. Sassaroli, M., Ching, Y., Argade, P. & Rousseau, D. L. (1988) *Biochemistry* **27**, 2496–2502.
16. Babcock, G. T. (1988) in *Biological Applications of Raman Spectroscopy*, ed., Spiro, T. G. (Wiley-Interscience, New York), Vol. 3, pp. 298–350.
17. Scheidt, W. R. & Lee, Y. J. (1987) *Struct. Bonding (Berlin)* **64**, 2–69.
18. Reed, C. A., Mashiko, T., Scheidt, W. R., Spartalian, K. & Lang, G. (1980) *J. Am. Chem. Soc.* **102**, 2302–2310.
19. Babcock, G. T., Vickery, L. E. & Palmer, G. (1976) *J. Biol. Chem.* **251**, 7907–7919.
20. Hille, R., Olson, J. S. & Palmer, G. (1979) *J. Biol. Chem.* **254**, 12110–12120.
21. Li, P. M., Gelles, J., Chan, S. I., Sullivan, R. J. & Scott, R. A. (1987) *Biochemistry* **26**, 2091–2095.
22. Fee, J. A., Mather, M. W., Springer, P., Hensel, S. & Buse, G. (1988) *Ann. NY Acad. Sci.* **550**, 33–38.
23. Wilkinson, G. W., Stone, F. G. A. & Abel, E. W., eds. (1982) *Comprehensive Organometallic Chemistry* (Pergamon, Oxford).
24. Cotton, F. A. & Wilkinson, G. W. (1988) *Advanced Inorganic Chemistry—A Comprehensive Text* (Interscience, New York), 5th ed.
25. Caughey, W. S., Smythe, G. S., O'Keeffe, D. H., Maskasky, J. E. & Smith, M. L. (1975) *J. Biol. Chem.* **250**, 7602–7622.
26. Sibbett, S. S. & Hurst, J. K. (1985) in *Biological and Inorganic Copper Chemistry*, Karlin, K. D. & Zubieta, J., eds. (Adenine, Guilderland, NY), pp. 123–141.
27. Deardorff, E. A., Carr, P. A. G. & Hurst, J. K. (1981) *J. Am. Chem. Soc.* **103**, 6611–6616.
28. Rossi, A. R. & Hoffman, R. (1975) *Inorg. Chem.* **14**, 365–374.
29. Woodruff, W. H., Dyer, R. B., López-Garriga, J. J., Einarsdóttir, Ó. & Killough, P. M. (1989) in *Proceedings of the 4th International Conference on Time-Resolved Vibrational Spectroscopy*, eds. Spiro, T. G. & Czernuszewicz, R. S. (Princeton Univ. Press, Princeton, NJ).
30. Woodruff, W. H., Einarsdóttir, Ó., Dyer, R. B., López-Garriga, J. J., Bagley, K. A., Atherton, S. J., Hubig, S. & Palmer, G. (1989) in *Proceedings of the VI International Conference on Energy and Electron Transfer*, eds. Fiala, J. & Pokorný, J. (Charles Univ. Press, Prague).
31. Ray, G. B., Copeland, R. A., Lee, C. P. & Spiro, T. G. (1990) *Biochemistry* **29**, 3208–3213.
32. Yoshikawa, S. & Caughey, W. S. (1990) *J. Biol. Chem.* **265**, 7945–7958.
33. Wikström, M., Krab, K. & Saraste, M. (1981) *Cytochrome Oxidase—A Synthesis* (Academic, New York).
34. Malmström, B. G. (1990) *Arch. Biochim. Biophys.* **280**, 233–241.
35. Chan, S. I. & Li, P. M. (1990) *Biochemistry* **29**, 1–12.